On the use of the GP-NARX model for predicting hysteresis effects of bolted joint structures

Rafael de Oliveira Teloli

UNESP - Universidade Estadual Paulista, Faculdade de Engenharia de Ilha Solteira, Departamento de Engenharia Mecânica, Av. Brasil, 56, Ilha Solteira, 15385-000, SP, Brasil

Luis G. G. Villani

UFES - Universidade Federal do Espírito Santo, Centro Tecnológico, Departamento de Engenharia Mecânica, Av. Fernando Ferrari, 514, Goiabeiras, Vitória, 29075-910, ES, Brasil

Samuel da Silva

UNESP - Universidade Estadual Paulista, Faculdade de Engenharia de Ilha Solteira, Departamento de Engenharia Mecânica, Av. Brasil, 56, Ilha Solteira, 15385-000, SP, Brasil

Michael D. Todd

UCSD - University of California San Diego, Department of Structural Engineering, 9500 Gilman Dr, La Jolla, CA, USA

Abstract

Structures joined by lap-joints can present complex nonlinear dynamic behavior as a function of the stress to which the lap-joint is subjected, including contact stiffness variations and softening, along with hysteresis effects related to frictional dissipation at the contact interface. Considering applications where the use of non-parametric models that depend only on input and output data is required, this work proposes and details the GP-NARX model's use to approximate systems' dynamics with hysteresis. Initially, the proposed model's predictive applicability is evaluated on a numerical application involving the Bouc-Wen oscillator with hysteretic damping. Then, this work proposes a GP-NARX model to describe the dynamics of the BERT benchmark, an experimen-

Email addresses: rafael.teloli@unesp.br (Rafael de Oliveira Teloli), luis.villani@unesp.br (Luis G. G. Villani), samuel.silva13@unesp.br (Samuel da Silva), mdtodd@eng.ucsd.edu (Michael D. Todd)

tal system that contains a symmetric double bolted joint that is nonlinearly dependent upon the applied excitation amplitudes, presenting as a friction joint's well-known softening effect. The structure also presents data variation related to the presence of uncertainties in the measurement process. Thus, to accommodate the experimental variability, the training step of the GP-NARX model considers several experimental realizations. The results indicate that GP-NARX can make accurate predictions of the response of both investigated applications, emphasizing its practical ability, where the confidence intervals of the proposed model were able to accommodate the experimental measurements.

Keywords: hysteretic systems, jointed structures, GP-NARX, uncertainties.

1. Introduction

In engineering structural design, the benefits of using assembled structures compared to monolithic ones lie in building complex, modular geometries, which can reduce the overall weight or even facilitate the replacement of damaged components [1]. Nevertheless, the transmission of movement in assembled components may occur nonlinearly due to the frictional contact between connected interfaces. Such nonlinearities are amplitude-dependent, i.e., their behavior depends upon the stress level to which the lap-joint is subject, and they are observed as variations in contact stiffness (softening effects) and damping induced by friction and partial slip (hysteretic effects) [2, 3]. Thus, to provide a greater understanding of jointed assemblies with the assessment of different vibration environments, predicting such systems' behavior is still a challenging topic of interest in the research community [4].

Finite element (FE) models are commonly used on an industrial scale (even millions of degrees of freedom) to predict energy dissipation and stress distribution of assembled structures. However, handling contact problems involves complex nonlinearities governed by micro and mesoscale parameters, e. g., geometry, roughness, and contact pressure [5], which considerably increases the complexity and computational cost of these numerical models. Some other nu-

merical tools have been developed in recent years to accelerate such simulations, including quasi-static modal analysis (QSMA) [6, 7, 8], reduced-order models (ROMs) [9, 10], and substructuring techniques based on the spatial decomposition of the structure in a local basis partitioned into linear and nonlinear subdomains, with the latter encompasses the region around the lap-type bolted joint [11, 12].

Although the advance in FE methods has been significant, some applications involving bolted joints, such as detection of bolt loosening for structural health monitoring (SHM) purposes [13, 14], require predictive models that demand relatively less-expensive computational cost while only relying on input and output data. Towards this objective, data-based models that do not depend directly on physical parameters to be identified, so-called black-box models, emerge as an alternative to model structures assembled by bolted joints, despite that they have been only slightly explored within this context or to identify hysteretic systems. Worden et al. (2007) [15] conducted a survey on identification techniques structured in grey and black-box approaches to predict friction effects present in a tribometer device by using, for instance, Nonlinear Autoregressive with eXogenous inputs (NARX) and neural networks models. Later, Worden and Barthorpe (2012) [16] proposed using a NARX structure with model parameters expanded into a non-polynomial basis function to identify the input-output process of a Bouc-Wen oscillator. Leva and Piroddi (2002) [17] presented a NARX-based modeling strategy to describe hysterical dynamic behavior for control purposes of magnetorheological dampers. Although the authors consider an approach that the NARX model is not polynomial, but that preserves linearity in its parameters, only one-step-ahead predictions were performed, in which those future output predictions depend on the previously real output measurements of the system under analysis. Then, to generalize polynomial NARX models for describing systems with hysteresis, Martins and Aguirre (2016) [18] introduced a new way to construct NARX models by using the concept of bounding functions that seek to encode the hysteresis loop into the structure of such models for estimating the data produced by a magne-

torheological damper. Noël et al. (2016) [19] proposed a framework to identify the dynamic behavior of a Bouc-Wen model benchmark based on the nonlinear state-space approach expanded into a nonlinear polynomial basis. However, a potential limitation of black-box models lies in the fact that the model structure should be carefully selected to reproduce the memory effect of hysteresis (input-output dependency [20]) while avoiding these models from being restricted to reproduce only output signals with the same characteristics used during their identification process.

In order to address the above-mentioned technical issues that black-box models may have in capturing hysteresis, this work aims to examine the GP-NARX model's benefits to predict the dynamic output signals from structures assembled by bolted joints. This model combines the machine learning Gaussian Process (GP) regression model with the NARX framework, providing a representation of the system of interest with natural probabilistic confidence intervals based on the model uncertainties. Inclusion of the confidence intervals makes the GP-NARX framework very suitable for decision processes, like those required in SHM applications. One of the main advantages of considering the GP-NARX model over other non-parametric models is that it considers the Bayesian inference to learn from the available data, which decreases the possibility of overparameterizing the nonlinear function responsible for mapping the output given a known input. Additionally, the inference is performed directly over the nonlinear function that describes the input-output relation, and not over model parameters. Therefore, it is a generalization of the Bayesian inference commonly used to estimate nonlinear models, based on models' parameters estimation. It is also important to highlight that, still in comparison with other non-parametric models, the model used in this work does not require prior knowledge of its structure (model order), as the classic approach made by NARX models [21]. This model should help monitor the hysteresis' fluctuations qualitatively caused by loss of torque applied in the bolts using indirect measurement data.

The paper is organized into five sections. First, section 2 introduces an

overview of the main aspects present in the identification of a GP-NARX model. To evaluate the applicability of the model to describe hysteretic systems, section 3 provides a numerical application of the GP-NARX model to approximate the outputs and hysteresis loops of the Bouc-Wen benchmark proposed by Noël and Schoukens (2016) [22]. Then, after establishing a methodology of model identification for the numerical benchmark with hysteresis, section 4 presents a practical application of the proposed model to reproduce the nonlinear dynamic behavior present in the first vibrating mode of a structure with a lap-type bolted joint connection, named as BoltEd stRucTure (BERT). Finally, section 5 reports the final remarks, main conclusions, and the path forward for future enquiry.

2. On the GP-NARX Model for Nonlinear Identification

GP-NARX is a nonlinear model class widely known in the machine learning community, with recent applications for identification purposes in engineering [23], including the wave force prediction on offshore structures [24] and the identification of the vertical flow of water in the cascaded tanks benchmark [25, 26]. This section begins with a brief description of the method, presenting the main aspects of identifying the GP-NARX model throughout subsection 2.1. For further details, the readers are invited to find more information in the literature made accessible. Then, subsection 2.2 outlines the step-by-step procedure to construct the GP-NARX model used in this work to reproduce the behavior of dynamic systems with a hysteresis.

2.1. GP-NARX model

A GP regression model is based on the idea of Bayesian inference; however, unlike the inference of the model's parameters used in classic Bayesian regression, the GP model considers the inference directly over functional space [27]. Thus, this model can be described as a generalization of a Bayesian regression method, in which any two or more observations that one wants to describe follow a multivariate Gaussian distribution [28]. In this sense, consider a general

regression problem to represent the process observations $y_i \in \mathbb{R}$ as

$$y_i = f(\mathbf{x}_i) + \varepsilon_i^{(y)}, \qquad i = 1, 2, \ldots, N \text{ samples} \tag{1}$$

where $f(\cdot)$ is a nonlinear function mapping the output to an input $\mathbf{x}_i \in \mathbb{R}^D$, and $\varepsilon_i^{(y)}$ is a stochastic variable representing inherent randomness in the observations. This randomness is assumed to be Gaussian distributed with zero mean

$$\varepsilon_i^{(y)} \sim \mathcal{N}\left(\varepsilon_i^{(y)} | 0, \sigma_y^2\right), \tag{2}$$

where σ_y^2 is the variance of the Gaussian noise observations.

In this work, in order to map the nonlinear effects related to the hysteresis, the NARX structure is considered as a nonlinear function that predicts the output y_i. Thus, the model's input $\mathbf{x}_i$ is formed by regression upon the excitation and output signals

$$\mathbf{x}_i = [y_{i-1}, ..., y_{i-n_y}, u_i, u_{i-1}, ..., u_{i-n_u+1}]^{\mathrm{T}}, \tag{3}$$

where u_i represents the oscillatory input signal at the i^{th} sample, and n_u and n_y are the number of regressors in the input and output signals, respectively.

Keeping in mind that the regression in equation (1) is represented by a Gaussian Process, the NARX structure $f(\mathbf{x}_i)$ is then formed by the assumption of a multivariate Gaussian prior distribution of zero mean

$$\mathbf{f} = f(\mathbf{x}_i) \sim \mathcal{N}(\mathbf{f}|0, \mathcal{K}), \tag{4}$$

resulting in the so-called GP-NARX model structure, where $\mathcal{K} \in \mathbb{R}^{N \times N}$ is the covariance matrix whose elements are described as $\mathcal{K}_{i,j} = k(\mathbf{x}_i, \mathbf{x}_j)$. The variable $k(\cdot, \cdot)$ is a covariance function, also named a kernel function, that models the dependence between the function values at different input samples. Due to the versatility in the GP-NARX model, the zero mean is assumed for simplicity.

The construction of the model function used for the regression process de-

pends directly on the knowledge acquired about the system of interest. Thus, assuming a set of training data available and making use of a simplified notation, one obtains

$$\mathscr{D} = (\mathbf{x}_i, y_i)_{i=1}^{N} \equiv (\mathcal{X}, \mathcal{Y}), \tag{5}$$

where $\mathcal{X} \in \mathbb{R}^{N \times D}$ is the regression matrix, and $\mathcal{Y} \in \mathbb{R}^{N}$ is the output vector. Since data observations for training contribute Gaussian white noise, the joint distribution of the training data and test samples, according to the prior distribution, is given by [27]

$$\begin{pmatrix} \mathcal{Y} \\ \mathbf{f}_* \end{pmatrix} \sim \mathcal{N}\left(\begin{pmatrix} \mathcal{Y} \\ \mathbf{f}_* \end{pmatrix} \middle| 0, \begin{bmatrix} \mathbf{K}(\mathcal{X}, \mathcal{X}) + \sigma_y^2 \mathbf{I} & \mathbf{K}(\mathcal{X}, \mathbf{x}_*) \\ \mathbf{K}(\mathbf{x}_*, \mathcal{X}) & \mathbf{K}(\mathbf{x}_*, \mathbf{x}_*) \end{bmatrix} \right), \tag{6}$$

where $\mathbf{f}_*$ denotes the predicted function at new input samples $\mathbf{x}_*$. $\mathbf{K}(\mathcal{X}, \mathcal{X})$ is the covariance matrix computed between the training input samples each other with elements $k(\mathbf{x}_i, \mathbf{x}_j)$, $\mathbf{K}(\mathcal{X}, \mathbf{x}_*)$ is the covariance matrix computed between the training and new input samples with elements $k(\mathbf{x}_i, \mathbf{x}_*)$ and $\mathbf{K}(\mathbf{x}_*, \mathcal{X}) = \mathbf{K}(\mathcal{X}, \mathbf{x}_*)^T$. Finally, $\mathbf{K}(\mathbf{x}_*, \mathbf{x}_*)$ is the covariance matrix between the new input samples and $\mathbf{I} \in \mathbb{R}^{N \times N}$ is an identity matrix.

Then, the Bayesian inference strategy is used to condition a posterior predictive distribution $\pi(\mathbf{f}_*|\mathbf{x}_*, \mathcal{X}, \mathcal{Y})$ over $\mathbf{f}_*$ based on the new available input, which gives the main relationship for the GP regression [27]

$$\pi(\mathbf{f}_*|\mathbf{x}_*, \mathcal{X}, \mathcal{Y}) \sim \mathcal{N}(\mathbf{f}_*|\mu_*, \sigma_*^2), \tag{7}$$

where the posterior predictive mean is given by

$$\mu_* = k(\mathbf{x}_*, \mathcal{X}) \left[\mathbf{K}(\mathcal{X}, \mathcal{X}) + \sigma_y^2 \mathbf{I}\right]^{-1} \mathcal{Y}, \tag{8}$$

and the posterior predictive variance is given by

$$\sigma_*^2 = k(\mathbf{x}_*, \mathbf{x}_*) - \mathbf{K}(\mathbf{x}_*, \mathcal{X}) \left[\mathbf{K}(\mathcal{X}, \mathcal{X}) + \sigma_y^2 \mathbf{I}\right]^{-1} \mathbf{K}(\mathcal{X}, \mathbf{x}_*). \tag{9}$$

Using equations (8)-(9), one can predict the new values of the function $\mathbf{f}_*$ as well as the values of $\mathbf{y}_*$ taking into account the model uncertainties, once both predictive distributions are similar. The variance σ_y^2 and the covariance function $k(\cdot,\cdot)$ need to be estimated based on the available data from the system under analysis. Many covariance functions were proposed over the years, with special attention to RBF, Exponential, Matérn 3/2, Matérn 5/2, Polynomial, Rational Quadratic, among others. The choice of the best kernel structure depends on the relations between the input/output data and the previous knowledge available on the system behavior. It is noteworthy that new kernel functions can also be proposed, just by considering a new formulation or even making use of a combination of existing functions [29]. In the context of this work, which explores the application of the GP-NARX model to represent hysteretic systems, the best results were achieved, considering the available data, by selecting a combination of two covariance kernels:

- Matérn 3/2:

$$k_1(\mathbf{x},\mathbf{x}') = \sigma_m^2 \left(1 + \frac{\sqrt{3}\,|\mathbf{x}-\mathbf{x}'|}{l}\right) \exp\left(-\frac{\sqrt{3}\,|\mathbf{x}-\mathbf{x}'|}{l}\right) \tag{10}$$

  where σ_m is the Matérn kernel variance and l the lengthscale.

- Cubic polynomial:

$$k_2(\mathbf{x},\mathbf{x}') = \sigma_p^2 \left[s(\mathbf{x}\mathbf{x}') + b\right]^3, \tag{11}$$

  where σ_p is the Polynomial kernel variance, s the scale and b the bias parameter.

Thus, the new additive kernel is given by

$$k(\mathbf{x},\mathbf{x}') = k_1(\mathbf{x},\mathbf{x}') + k_2(\mathbf{x},\mathbf{x}'). \tag{12}$$

Based on the unknown variables in the kernel, a vector of hyperparameters

may be defined as $\boldsymbol{\Theta} = \left[\sigma_m^2, l, \sigma_p^2, s, b, \sigma_y^2\right]$ and then estimated by conducting a maximization of the marginal log-likelihood of the observed data [30]

$$\log \pi(\mathcal{Y}|\mathcal{X}, \boldsymbol{\Theta}) = -\frac{1}{2}\log|\mathbf{K} + \sigma_y^2\mathbf{I}| - \frac{1}{2}\mathcal{Y}^{\mathrm{T}}(\mathbf{K} + \sigma_y^2\mathbf{I})^{-1}\mathbf{y} - \frac{N}{2}\log(2\pi). \quad (13)$$

Such a maximization procedure is performed using a gradient method, and the optimum model is used to predict new outputs as a consequence of new inputs. The GP-NARX model can describe a wide variety of structural dynamic behavior, taking advantage of its capability to consider modeling uncertainties and predicting the trend curves of outputs with probabilistic confidences.

The GP-NARX model will be used as a surrogate model to predict the hysterical behavior present in complex systems dynamics. As mentionated previously, the advantage of dealing with the GP-NARX model when compared to the classic NARX model [21] lies in the possibility of estimating the nonlinear relation between the regressors and the output based directly on the inference over the training data, which is a feature of GP regression, only by knowing the maximum number of input/output lags (n_y and n_u) [24].

2.2. Identification framework

The identification workflow proposed herein may be stated as follows:

- *Step 1: Data acquisition*

Systems with hysteresis present more pronounced nonlinear energy dissipation, which can be visualized through the opening of the hysteresis loops, increasing the response amplitude [6]. Depending on the excitation amplitude applied, these systems also present changes in their resonant frequencies due to hardening or softening effects. In these circumstances, identifying the GP-NARX model is conducted considering training data generated by swept sine excitation tests in the resonant frequency vicinity. These tests were also used in the *Model verification* step, but considering different excitation amplitudes from those used during the *Model training* step. Stationary sinusoidal testing and white noise signals with several excitation amplitudes were considered to

validate the proposed GP-NARX model. In numerical simulations it is interesting to add some synthetic white noise, avoiding overparameterization and making the inversion of the matrix $\left[\mathbf{K}(\mathcal{X},\mathcal{X})+\sigma_y^2\mathbf{I}\right]$ easier when strongly correlated training data is considered.

- *Step 2: Model training*

This step comprises the optimization of hyperparameters $\boldsymbol{\Theta}$ by maximizing the marginal log-likelihood from equation (13) and also the estimation of the maximum number of input/output lags. Based on the training data $(\mathcal{X},\mathcal{Y})$, a surface involving the number of lags and the output fit measured at each combination of lags is constructed. The model-fit, which corresponds to the mean relative square error (MSRE) metric, is evaluated by the following formulation

$$fit\,[\%] = 100 \times \left(1 - \sqrt{\frac{\sum_{i=1}^{N} \left(y_{\mathrm{exp,i}} - \mu(\hat{y}_i)\right)^2}{\sum_{i=1}^{N} y_{\mathrm{exp,i}}^2}} \right), \tag{14}$$

where $y_{\mathrm{exp,i}}$ is the experimental output signal and $\mu(\hat{y}_i)$ is the model mean output signal, both at the i^{th} instant of time. With the surface $(n_y \times n_u \times fit)$ estimated, the number of lags is chosen in the region that guarantees the best value of fit using a minimal number of lags. Of course, using a different output signal in the lag estimations from the one used in the model training step produces a better description of the system's dynamics.

- *Step 3: GP-NARX model verification and validation*

Once the model with the lags and hyperparameters has been defined, the model's predictive capability must be assessed. The reader will see that when we consider *infinite-step-ahead* prediction or *model predicted output* [21], those future output predictions depend on the previously predicted one that is approximated as a Gaussian random variable, defined by its mean μ_y and variance σ_y^2.

As a consequence, the GP-NARX formulation is affected by the backpropagation of the model uncertainties. Depending on the covariance function chosen, the backpropagation of the uncertainties may be computed analytically [31]. However, for a more general formulation based on the model-predicted output as used in this paper, Monte Carlo simulations are instead used to propagate all the model uncertainties, using the estimated Gaussian distribution [32].

3. Numerical Assessment of the GP-NARX model: The Bouc-Wen Benchmark

This section introduces the use of the GP-NARX model first in a numerical application involving the Bouc-Wen benchmark, which is given by [22]

$$m\ddot{y}(t) + c\dot{y}(t) + ky(t) + \mathcal{Z}(y,\dot{y}) = u(t) \tag{15}$$

$$\dot{\mathcal{Z}}(y,\dot{y}) = \alpha\dot{y}(t) - \beta\left(\gamma|\dot{y}||\mathcal{Z}(y,\dot{y})|^{\nu-1}\mathcal{Z}(y,\dot{y}) + \delta\dot{y}(t)|\mathcal{Z}(y,\dot{y})|^{\nu}\right), \tag{16}$$

where m [kg], c [Ns/m] and k [N/m] are the mass, damping and stiffness coefficients, respectively, and α [N/m], β, γ [m^{-1}], δ [m^{-1}], and ν are the Bouc-Wen model parameters. Additionally, $\ddot{y}(t)$ [$\mathrm{m/s}^2$], $\dot{y}(t)$ [m/s], and $y(t)$ [m] are the acceleration, velocity, and displacement, respectively, for an excitation input $u(t)$ [N]. $\mathcal{Z}(y,\dot{y})$ [N] represents the hysteretic restoring force which obeys the ordinary differential equation (16) of $\dot{\mathcal{Z}}(y,\dot{y})$ [N/s]. This model presents challenging issues for conventional system identification techniques such as the existence of a hysteretic force with multiple solutions (non-smooth nonlinearity), memory dependency, the presence of multiple harmonics in the oscillator output, among others. Further details involving the hysteretic benchmark are also addressed by Bajrić and Høgsberg (2018) [33], Rebillat and Schoukens (2018) [34], Teloli et al. (2019) [35] and Miguel et al. (2020) [36].

Table 1 shows the model parameters selected according to [22]. All simulations with the benchmark presented in this work use a sampling frequency of 750 Hz. The oscillator's responses were obtained through a numerical integration scheme with the 4^{th} order Runge-Kutta method and variable time-step.

m [kg]	c [Ns/m]	k [N/m]	α [N/m]	β	γ [m^{-1}]	δ [m^{-1}]	ν
2	10	5×10^4	5×10^4	1×10^3	0.8	-1.1	1

Table 1: Bouc-Wen benchmark parameters [22].

It should be pointed out that the objective herein is to predict the Bouc-Wen oscillator's response described in equations (15) and (16) bounded by probabilistic confidence intervals produced by the GP-NARX model. This work is different from that proposed by Bhattacharyya et al. (2020) [37], who consider a stochastic version of the Bouc-Wen oscillator described by random variables and then use the Kriging-NARX model to predict its response. Unlike the GP-NARX version, which takes into account the inference over functions, the Kriging-NARX model considers the stochastic expansion of the NARX model's coefficients and then becomes not useful to describe dynamic systems subject to white noise excitation for predicting statistically characterized responses.

3.1. Model training

One of the main aspects to be considered in constructing a numerical model is related to the training data and how these are conditioned to the excitation signal applied in the dynamic system. Some key elements should be highlighted within this context, such as the system operating range, vibration modes of interest, whether the nonlinearity is amplitude-dependent or frequency-dependent, and so on. To encode and reproduce this nonlinearity from the hysteretic oscillator, the GP-NARX model is constructed considering swept sine tests in the resonance frequency vicinity. Such tests provide an attractive, cost-effective ratio between the excitation level amplitude, frequency control, and testing time (particularly for practical applications).

Thus, the training data $(\mathcal{X}, \mathcal{Y})$ used for the GP-NARX model inference and estimation of hyperparameters Θ consist of a pair of responses of the Bouc-Wen oscillator for a swept sine test applied from 5 up to 150 Hz, with input amplitude levels of 10 and 80 N (low and high) and both with a frequency increase rate of $\approx$ 53 Hz/s. Additionally, to emulate experimental conditions

during the training, verification, and validation steps of the GP-NARX model construction, white noise was added to the response data, considering 10% of the total energy of the response signal for input with the lowest level of excitation amplitude (10 N).

In the lag optimization procedure, the GP-NARX model is estimated several times, considering different combinations of n_u and n_y. In contrast, the model performance is measured using Eq. (14), taking into account the same swept sine test, with an input amplitude level of 50 N (medium). Using a different amplitude signal improves the procedure, ensuring that the number of lags will be satisfactory in different motion regimes. Figure 1 presents the lags optimization surface with emphasis on the optimal values found, which correspond to the regression order of $n_y = 20$ lags in the output and $n_u = 17$ lags in the input for a fit of 92.4%. Then, having defined the model structure, the next step lies in verifying its performance to reproduce the Bouc-Wen oscillator's responses by assuming sweep sine signals with the same characteristics and several excitation amplitudes.

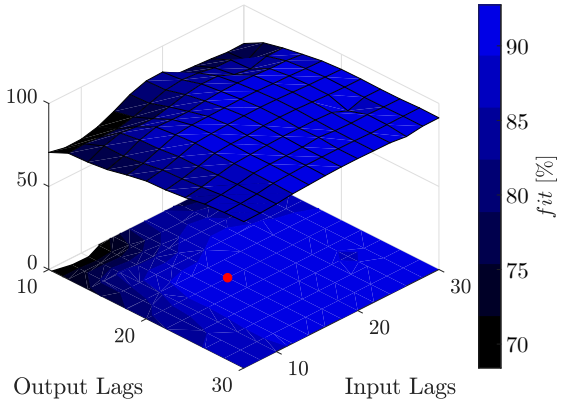

Figure 1: Lags optimization surface $n_y \times n_u \times fit$. The optimal value of the lags (•) corresponds to 20 lags in the output and 17 lags in the input for a fit of 92.4 %.

3.2. GP-NARX model verification and validation

Throughout this subsection, all the model statistics were estimated considering the backpropagation of uncertainties through Monte Carlo simulations with

1024 samplings, ensuring that all the model uncertainty is considered in the predictions. Additionally, all figures consider 99% statistical confidence bounds.

Figure 2 presents the assessment of the GP-NARX model, considering a low level of excitation amplitude (10 N). Figs. 2(a) and (b) depict the model-predicted output in direct comparison with the displacement response of the Bouc-Wen model. The results show that the confidence bounds were able to accommodate the model's response, with a narrower band in the resonance region than near the end of the signal ($\approx$ 1.5 and 2 seconds), primarily due to signal-to-noise. Figure 2(c) shows a close-up view of the power spectrum density (PSD) of responses over a frequency range of $5 - 150$ Hz, evidencing that the model-predicted output carries the same frequency content as the Bouc-Wen oscillator response. All spectra presented throughout this subsection for sweeping sine tests have been calculated with the Welch's periodogram considering a rectangular window over the entire signal length. Figure 2(d) exhibits the numerically integrated hysteresis loop compared to the predicted one. Although the hysteresis loop is almost closed to a low level of excitation amplitude, the black-box model can accommodate the system's accuracy with hysteresis, having the model mean output enclosing substantially the same area as the Bouc-Wen oscillator in the restoring force *versus* displacement plane.

Figures 3 and 4 exhibit the model-predicted output with 99% of statistical confidence in comparison with Bouc-Wen data for two levels of excitation amplitude, medium (50 N) and high (80 N), respectively. From these figures, note that the GP-NARX model can reproduce the dynamics of the Bouc-Wen's oscillator even at higher excitation amplitudes, where the effects of nonlinear energy dissipation are evidenced through the pronounced opening of hysteresis loops. A comparison between the spectra of Figs. 2(c), 3(c) and 4(c) shows that the model is able to follow the hardening effect present in the Bouc-Wen oscillator ($\gamma + \delta < 0$) [38], which is characterized by increasing the resonance frequency for higher response amplitudes.

It is also important to note that the confidence bounds for a higher excitation level are narrower about the mean prediction. This is due to the lower signal-

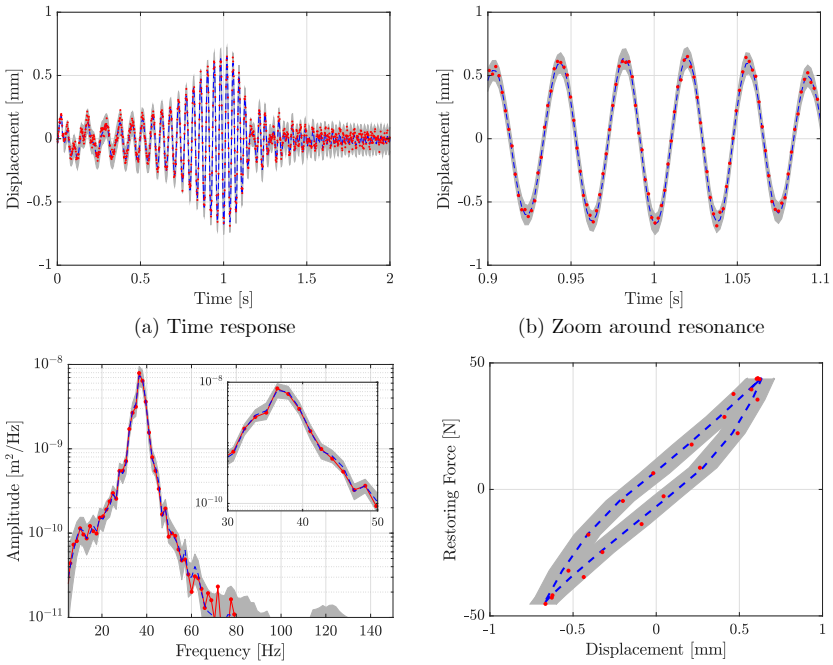

(a) Time response (b) Zoom around resonance

(c) PSD (d) Hysteresis loop

Figure 2: Verification of the GP-NARX model for low excitation amplitude (10 N) considering a swept sine test. ▒ represents the 99% model-predicted output confidence bands, —— is the model response mean and • represents the Bouc-Wen data obtained by numerical integration.

to-noise in higher amplitude signals and the fact that the model uncertainty is lower in regions close to the training data.

In general, the construction of black-box models may involve some pitfalls. One of them is that these models can be over-conditioned by the training data used in their construction, such as the Kriging-NARX model proposed by Bhattacharyya et al. (2020) [37]. In other words, this might mean that a model identified to describe a nonlinear system based on sinusoidal inputs as training data may only be able to reproduce the responses of such a system that feature the same characteristics in the input. In this context, this subsection discusses the robustness and validity of the GP-NARX model in reproducing the hysterical behavior of the Bouc-Wen benchmark assuming inputs different from those used in its construction, such as a stationary sinusoidal and a random phase multi-sine excitation [22] for low (10 N), medium (50 N) and high

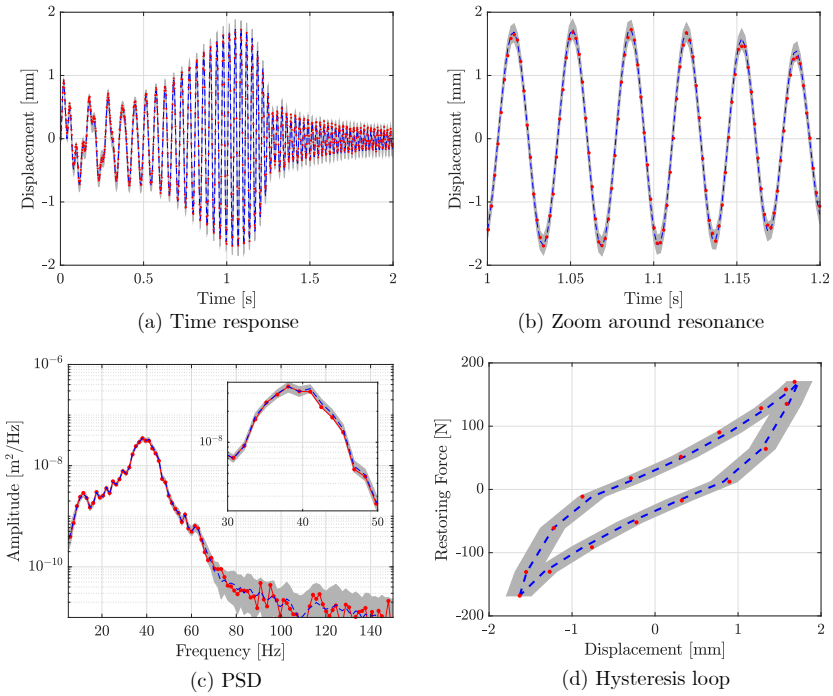

(a) Time response (b) Zoom around resonance

(c) PSD (d) Hysteresis loop

Figure 3: Verification of the GP-NARX model for medium excitation amplitude (50 N) considering a swept sine test. ▓ represents the 99% model-predicted output confidence bands, — is the model response mean and • represents the Bouc-Wen data obtained by numerical integration.

(80 N) amplitude levels.

Figures 5, 6 and 7 provide an overview of the model-predicted outputs in comparison with Bouc-Wen data for three levels of excitation amplitude, low (10 N), medium (50 N) and high (80 N), respectively, for a sinusoidal input $u(t) = A\sin(2\pi\omega_n t)$ with excitation frequency at the linear resonance $\omega_n = 35.59$ Hz. On the one hand, for a low excitation amplitude, Fig. 5 depicts that the Bouc-Wen system operates with reduced severity of nonlinear effects, showing through the Fig. 5(c) that the spectrum of responses has no contributions of odd higher-order harmonics, e.g., third, fifth and seventh-order harmonics. Welch's periodogram with a Hanning window every $N = 2^9$ samples was used to reveal this. On the other hand, for medium and high excitation amplitudes, Figs. 6(c) and 7(c) emphasize the GP-NARX model's ability to reproduce nonlinear distortions present in the Bouc-Wen's system response while

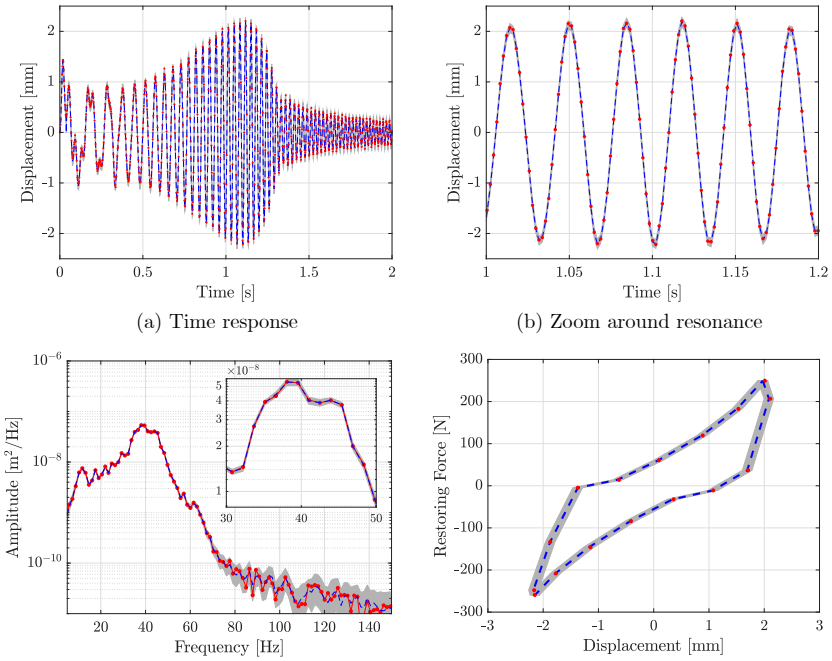

(a) Time response (b) Zoom around resonance

(c) PSD (d) Hysteresis loop

Figure 4: Verification of the GP-NARX model for high excitation amplitude (80 N) considering a swept sine test. ▒ represents the 99% model-predicted output confidence bands, —— is the model response mean and • represents the Bouc-Wen data obtained by numerical integration.

accommodating the odd harmonics of the output within the confidence bands.

The Bouc-Wen model carries the rate-independent hysteresis property, which means that for the same excursion interval of the output bounded between amplitudes $y_{\min} \leqslant y(t) \leqslant y_{\max}$, the restoring force $\mathcal{Z}(t)$ of the system will present the same hysteresis loop when it is excited by a $T-$periodic input signal with a loading-unloading regime defined in a period $T \in \mathbb{R}^+$ [39, 35]. Therefore, note that the excursion intervals on displacement present in the hysteresis loops of Figs. 5(d), 6(d) and 7(d) are approximately the same presented in Figs. 2(d), 3(d) and 4(d), respectively; this shows that the GP-NARX model is able to reproduce the rate-independent hysteresis property through the model-predicted outputs for input signals with a harmonic characteristic, also representing both system responses with a similar confidence bands, e. g., Figs. 5(d) and 2(d).

The model-predicted outputs for a random phase multi-sine excitation [22,

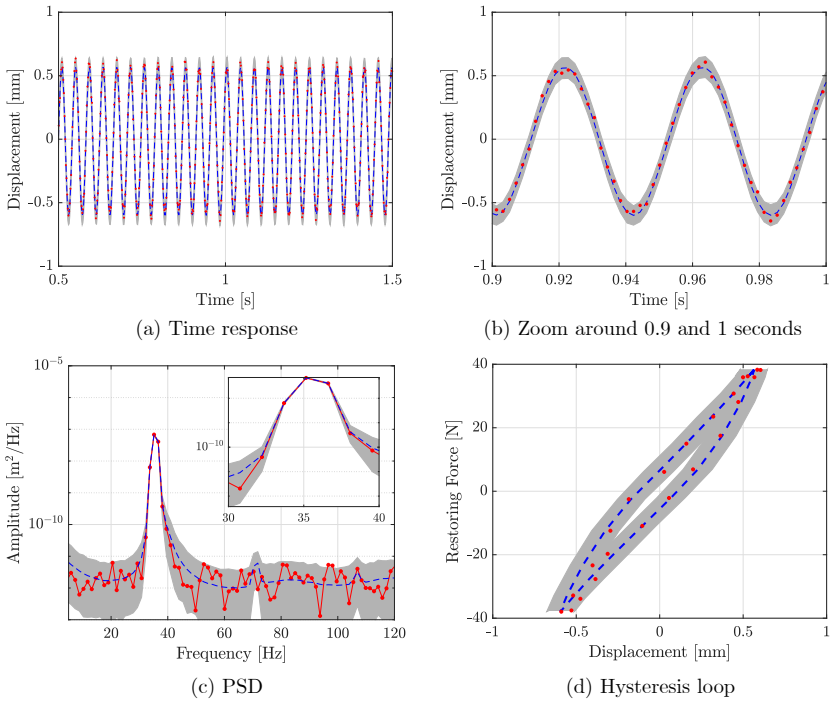

(a) Time response (b) Zoom around 0.9 and 1 seconds

(c) PSD (d) Hysteresis loop

Figure 5: Validation of the GP-NARX model for low excitation amplitude (10 N) considering a sinusoidal input with excitation frequency at the linear resonance $\omega_n = 35.59$ Hz. ▓ represents the 99% model-predicted output confidence bands, —— is the model response mean and • represents the Bouc-Wen data obtained by numerical integration.

19] over a frequency range of $5 - 150$ Hz are shown in Figs. 8, 9 and 10, considering low (10 N), medium (50 N) and high (80 N) excitation amplitudes, respectively. As the model is used to predict the system behavior for random characteristics that are substantially different from the data observed in training, it should be stressed that the further away from the training data region one wants to make predictions using the model estimated (e.g., using a random excitation), more uncertainty will be present in the model's output. This means that the model will not necessarily make wrong predictions far from the training data, but the forecasts will be more uncertain, and in some situations, the mean prediction value may become unrepresentative. For all the levels of excitation considered, the confidence bands of the model-predicted outputs accommodate the responses from the Bouc-Wen oscillator.

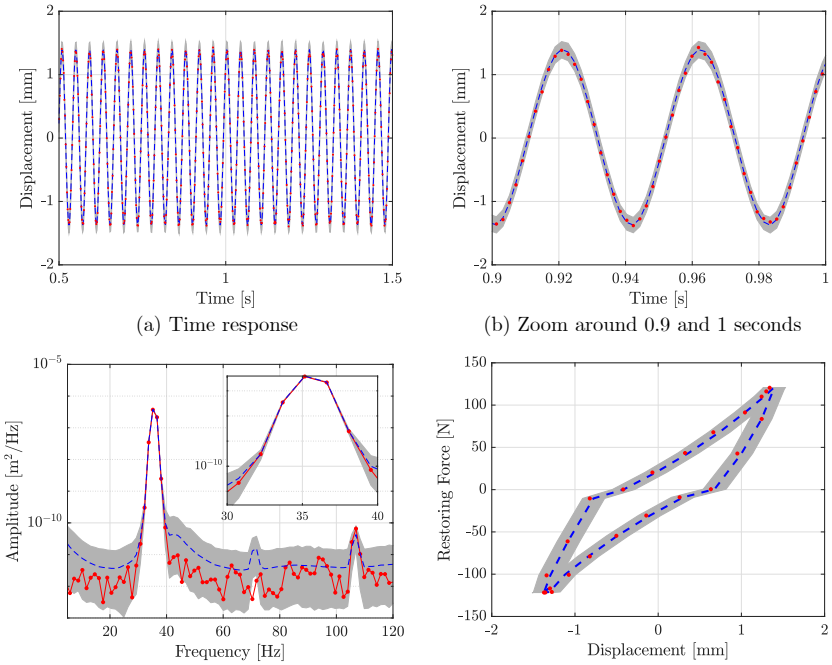

(a) Time response (b) Zoom around 0.9 and 1 seconds

(c) PSD (d) Hysteresis loop

Figure 6: Validation of the GP-NARX model for medium excitation amplitude (50 N) considering a sinusoidal input with excitation frequency at the linear resonance $\omega_n = 35.59$ Hz. ▓ represents the 99% model-predicted output confidence bands, —— is the model response mean and • represents the Bouc-Wen data obtained by numerical integration.

4. Experimental Assessment of the GP-NARX Model: The BoltEd stRucTure (BERT) Benchmark

4.1. Description of the experimental setup

This section considers the BoltEd stRucTure (BERT) benchmark[1] shown in Fig. 11 as a bolted jointed structure to test the robustness of the GP-NARX model when dealing with experimental hysteretic systems. The experimental setup consists of two aluminum beams assembled in a clamped-free boundary condition, each with dimensions of $270 \times 25.4 \times 6.35$ mm and connected by two M5 bolts, spaced along a length of 40 mm, with a tightening torque of 5 Nm. An electromagnetic Modal Shop 2400E shaker is placed at 85 mm from the clamped end to minimize shaker–structure interaction [40]. For observability purposes,

[1]Data available on https://github.com/shm-unesp/DATASETBOLTEDBEAM

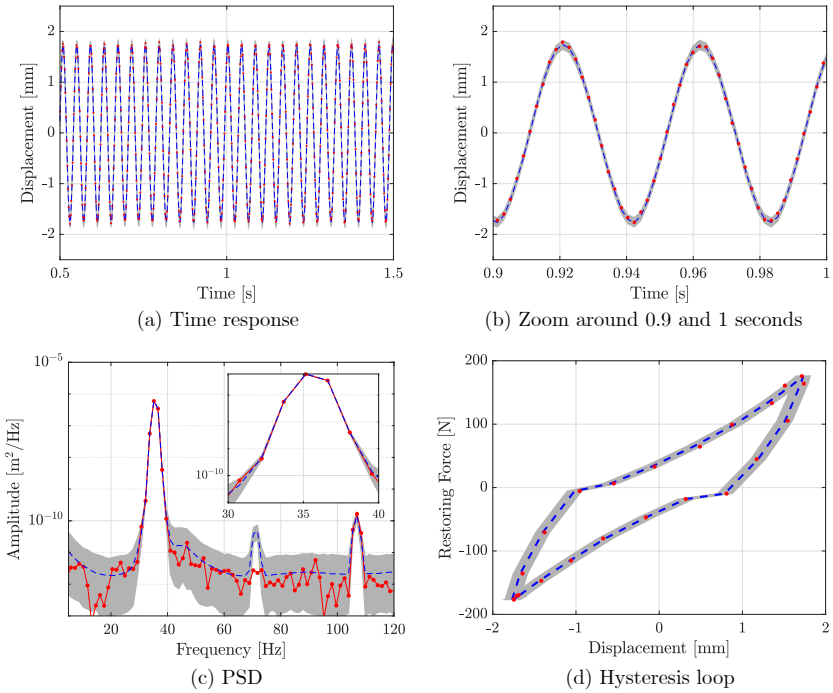

(a) Time response (b) Zoom around 0.9 and 1 seconds

(c) PSD (d) Hysteresis loop

Figure 7: Validation of the GP-NARX model for high excitation amplitude (80 N) considering a sinusoidal input with excitation frequency at the linear resonance $\omega_n = 35.59$ Hz. ▓ represents the 99% model-predicted output confidence bands, ——— is the model response mean and ● represents the Bouc-Wen data obtained by numerical integration.

since this work considers the first mode of vibration of the structure in interest, all measurements considered herein were made at the free end of the assembled beam by a laser vibrometer Polytec OFV-525/5000S. The data acquisition was performed by an LMS SCADAS system using a sampling frequency of 1024 Hz. The input signals applied to excite the structure were conducted, assuming different voltage amplitude levels applied to the shaker amplifier, from low to high values (0.05, 0.10, 0.15 and 0.20 [V]). Further details regarding the excitation are addressed in the following subsections. Figure 11 shows the schematic top view of the test-rig.

Figure 12 illustrates a preliminary analysis of the nonlinear behavior of the BERT benchmark through the frequency response curves around its first resonant frequency (≈ 18.8 Hz). Figure 12(a) corresponds to the magnitude plot of the receptance, which was estimated from the structures' response to the swept

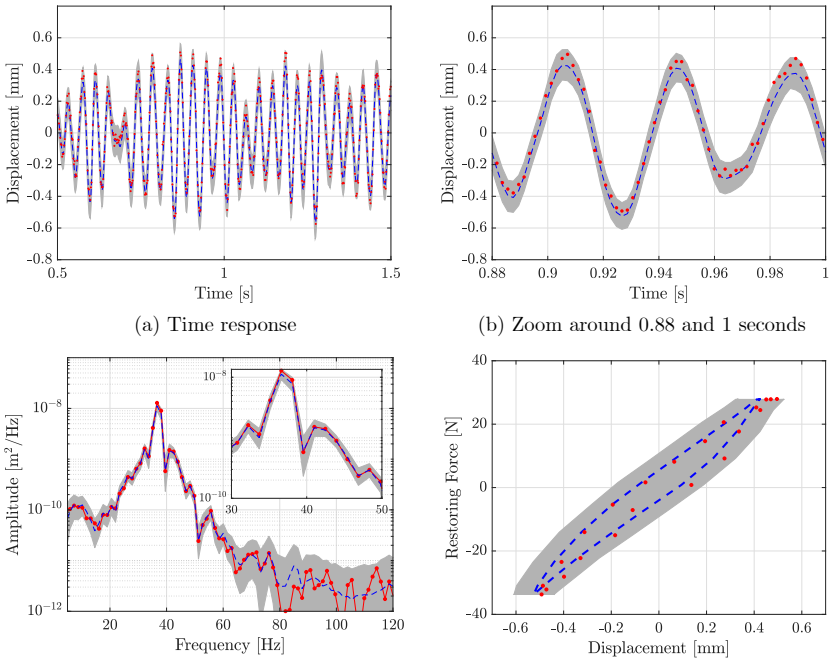

(a) Time response (b) Zoom around 0.88 and 1 seconds

(c) PSD (d) Hysteresis loop

Figure 8: Validation of the GP-NARX model for low excitation amplitude (10 N) considering a random phase multisine excitation. ▓ represents the 99% model-predicted output confidence bands, ——— is the model response mean and • represents the Bouc-Wen data obtained by numerical integration.

sine test from 0 up to 40 Hz (sweep rate of 5 Hz/s) collected with 16384 samples and a burst of 50 %, regarding low (0.05 V), medium (0.10 V) and high (0.20 V) levels of amplitude. One can verify that the FRFs do not overlay for different input levels, exhibiting distortions, changes in resonance frequency, and a more significant attenuation of vibration amplitude for higher excitation levels.

In a complementary way, Fig. 12(b) exemplifies the frequency response curve of the assembled structure obtained from stepped sine tests sweeping up from 3 to 23 Hz, with incremental steps of 0.1 Hz and 32 seconds of oscillations to ensure steady-state condition at each excitation frequency. It is noteworthy that, as well as several bolted jointed structures, the BERT benchmark presents amplitude-dependent nonlinearity, with a decrease in the value of its resonant frequency when increasing the input amplitude. This illustrates the fact that the lap-joint inevitably softens the total rigidity of the system. Recently, Teloli

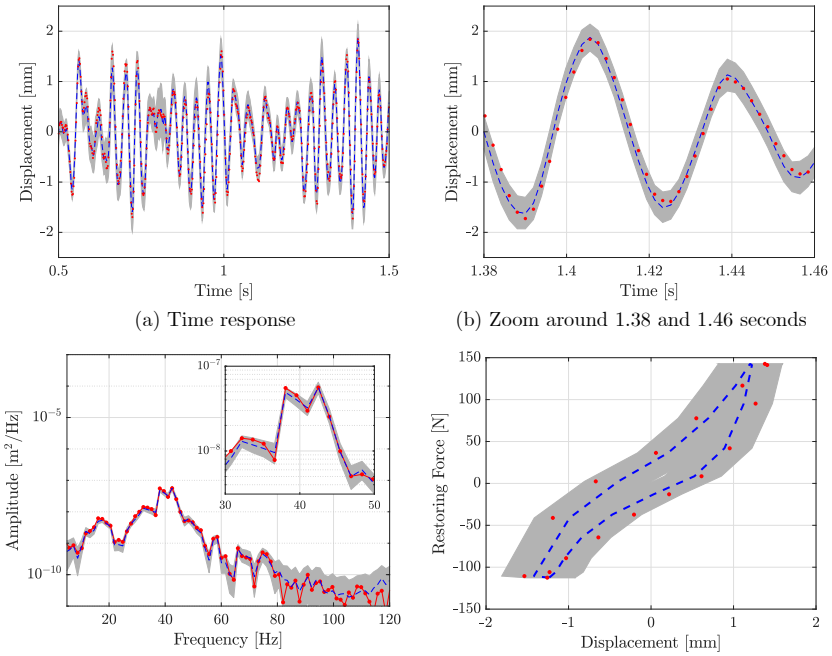

(a) Time response (b) Zoom around 1.38 and 1.46 seconds

(c) PSD (d) Hysteresis loop

Figure 9: Validation of the GP-NARX model for medium excitation amplitude (50 N) considering a random phase multisine excitation. ▓ represents the 99% model-predicted output confidence bands, ——— is the model response mean and ● represents the Bouc-Wen data obtained by numerical integration.

et al. (2021) [41] demonstrated that the behavior of the benchmark around its first mode of vibration could be well approximated by a stochastic version of the Bouc-Wen oscillator.

Figure 13 exemplifies the data fluctuation on frequency response curves considering several experimental measurements and is shown with 99% statistical confidence bounds. The experimental measurements were conducted over different days, and only the tightening torque in the joint connection was controlled after each experimental realization.

4.2. Model training

Following the same identification framework discussed in section 2.2 and exemplified on the numerical benchmark of section 3, the training data set $(\mathcal{X}, \mathcal{Y})$ used for the GP-NARX model inference and estimation of hyperparameters Θ

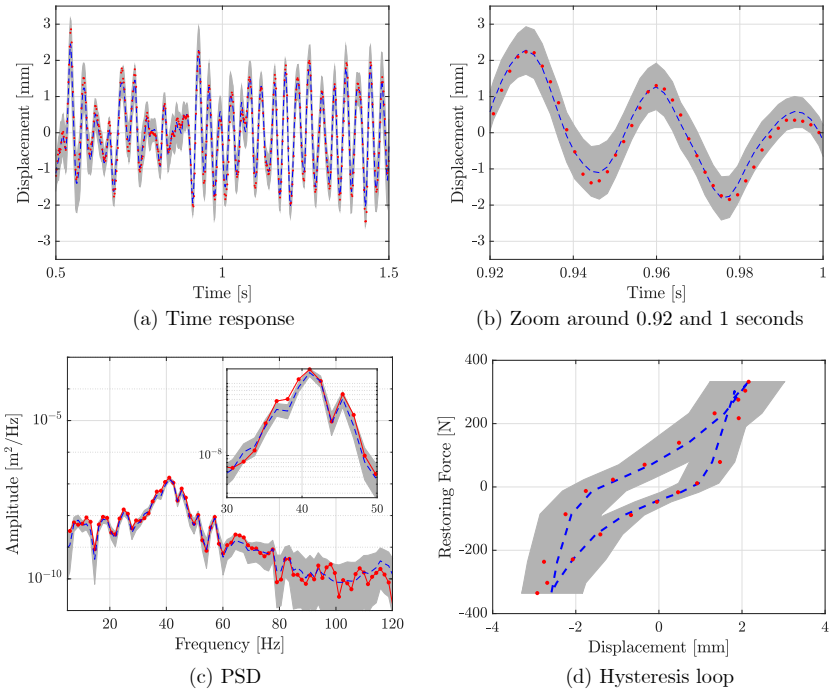

(a) Time response (b) Zoom around 0.92 and 1 seconds

(c) PSD (d) Hysteresis loop

Figure 10: Validation of the GP-NARX model for high excitation amplitude (80 N) considering a random phase multisine excitation. ▓ represents the 99% model-predicted output confidence bands, ——— is the model response mean and • represents the Bouc-Wen data obtained by numerical integration.

consist of a pair of experimental responses collected from the BERT system for the swept sine test described previously and considering amplitude levels of 0.05 and 0.20 V (low and high), respectively. In this work, the shaker amplifier's voltage signal is used as input data for training, verification, and validation of the GP-NARX model. This approach is considered as excitation once this signal is constant over a frequency range [42].

Also, to take into account the data fluctuation observed in Fig. 13 during the construction of the GP-NARX model, the training data consider data points randomly chosen from 50 available experimental realizations, using only samples of the time data acquired around the region of maximum response amplitudes due to the presence of resonance. This procedure is performed to reduce the computational cost necessary in the *Model training* step, considering only the part of the data that has the most predominating dynamics. Additionally, using

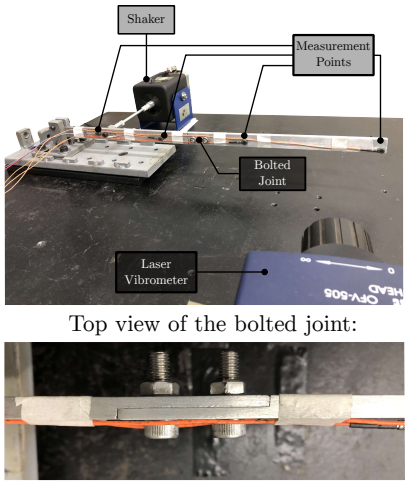

(a) Experimental setup

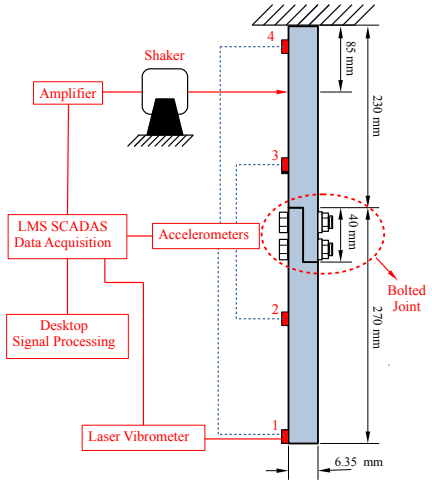

(b) Schematic top view of the experimental setup.

Figure 11: BERT setup and the schematic representation illustrating the clamped-free beam conveying a bolted joint connection.

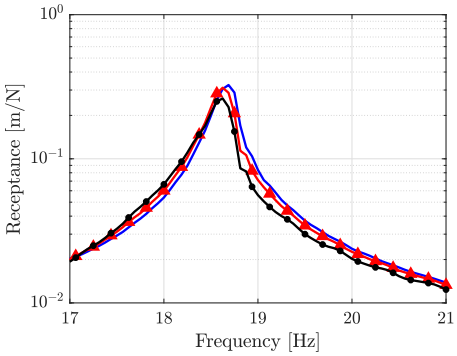

(a) Magnitude plot of the receptance.

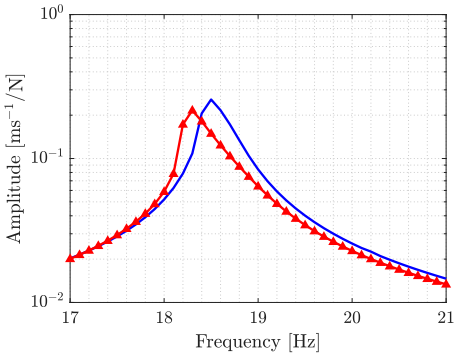

(b) Experimental frequency response curve for a stepped sine test.

Figure 12: Frequency response curves for different excitation amplitudes: —— is low (0.05 V), △ medium (0.10 V), and ○ high (0.20 V) amplitude levels.

this strategy, the model can predict the experimental uncertainty related to the variability from one realization to another.

Figure 14 presents the surface $n_y \times n_u \times fit$ [%] resulting from the GP-
395 NARX model lags optimization procedure considering signals from the swept sine test for an input amplitude of 0.10 V, which was used to improve the model performance, as mentioned above. It was found that optimal values of 16 lags

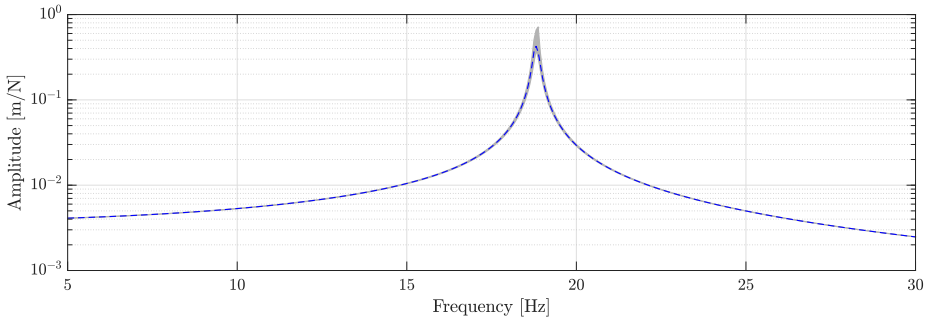

(a) Low level of excitation amplitude (0.05 V).

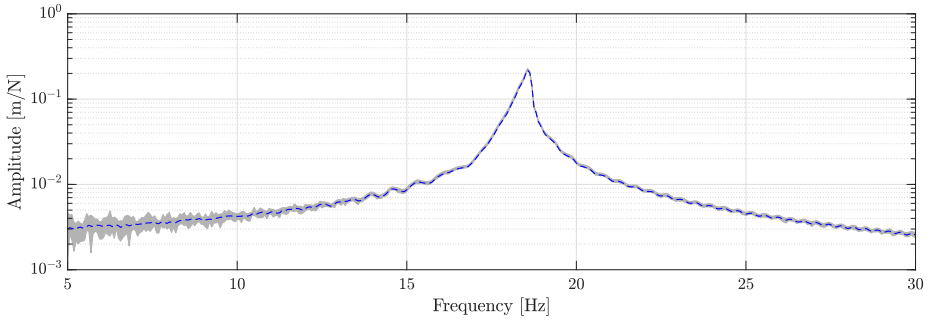

(b) High level of excitation amplitude (0.20 V).

Figure 13: Variation of the Frequency Response Function calculated for different excitation amplitudes with 99% of confidence bands. ▒ represents the confidence bands, whereas — is the mean values.

in the output and 10 lags in the input produced a fit of 96.1%.

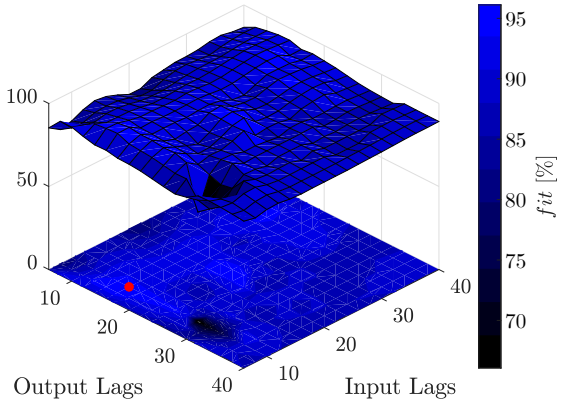

Figure 14: Lags optimization surface $n_y \times n_u \times fit$. The optimal value of the lags (•) corresponds to 16 lags in the output and 10 lags in the input for a fit of 96.1 %.

4.3. GP-NARX model verification and validation

To ensure convergence in estimating the model's statistical properties, all practical application results assume the backpropagation of the uncertainties considering 4096 Monte Carlo simulations.

The model verification is presented through Figs. 15, 16 and 17 whereby the GP-NARX model-predicted outputs are compared to the BERT benchmark's experimental results for low (0.05 V), medium (0.10 V) and high (0.20 V) levels of excitation amplitude, respectively. The black-box model presents good agreement with the experimental measurements since the model training step was conducted regarding these curves. The confidence bands accommodate several experimental realizations, which indicates that the model can make accurate predictions of the structure's behavior and response, even in the presence of nonlinear effects and data variability. Figures 15(c), 16(c) and 17(c) show that even with the increase in the excitation amplitude, an accurate fit of the frequency components of the experimental responses is achieved by the model.

Nevertheless, special attention is given to Figs. 15(d), 16(d) and 17(d), which present a comparison between the hysteresis loops obtained from the model response and those obtained from the experimental data. It can be seen that the mean response of the model can capture the evolution of the experimental data in the restoring force $\times$ displacement plane. It should be stressed that the restoring force considered in this comparison represents the projection of all nonlinear forces actuating on the first vibrating mode of the assembled structure around the resonance region (maximum amplitude).

Different input conditions are then tested from data that were not used to infer the model's parameters to validate the proposed model. Figure 18 depicts the model-predicted output considering the swept sine test with excitation amplitude at 0.15 V. For this excitation with intermediate amplitude between medium and high levels, the model showed it was able to reproduce the experimental measurements well. Although some points regarding the experimental realizations have exceeded the limits of the confidence bounds, which is apparent in the 18(d) concerning the hysteresis loops, there are no regions where the

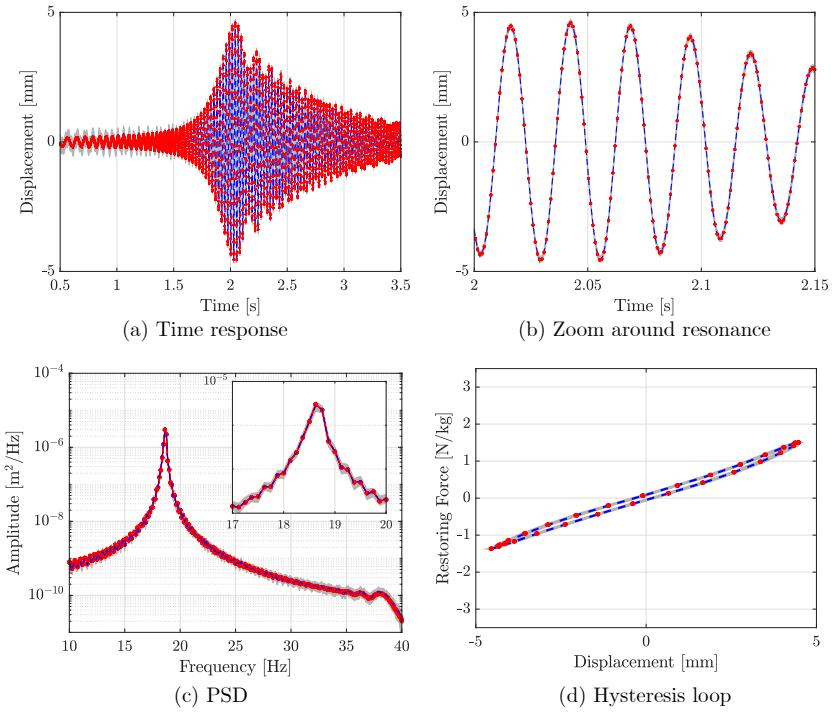

(a) Time response (b) Zoom around resonance

(c) PSD (d) Hysteresis loop

Figure 15: Verification of the GP-NARX model for low excitation amplitude (0.05 V) considering a swept sine test. ▓ represents the 99% model-predicted output confidence bands, —— is the model response mean and • represents ten experimental realizations.

dynamics visualized in the experiment are different from that predicted by the model.

Furthermore, in the context of model validation, the GP-NARX model-predicted output for a sinusoidal excitation with an amplitude level of 0.15 V and conducted close to the first resonance frequency (18 Hz) of the test-rig is shown in Fig. 19. From the PSD of the experimental response of the bolted structure present in Fig. 19(c), note that the numerical model can reproduce in its response the presence of multiple harmonics (2 and 3 times the fundamental frequency) that are also found in the experimental response. Although it overestimates the third-order harmonic component, the model is suitable to represent the nonlinearities of even and odd harmonic order associated with the assembled structure's behavior. Then, the GP-NARX model brings forward the hysteresis curves predicted in Fig. 19, which illustrates that almost the same energy dis-

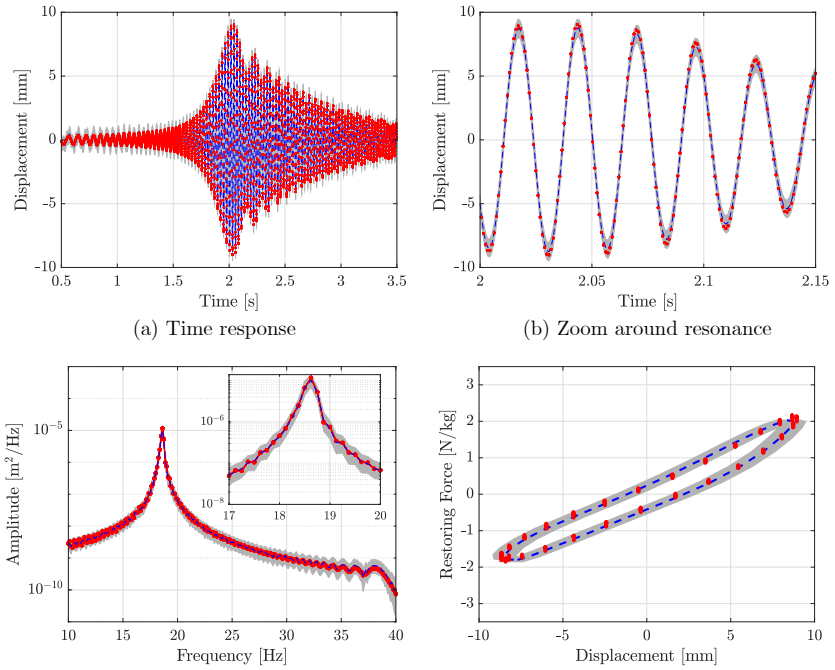

(a) Time response (b) Zoom around resonance

(c) PSD (d) Hysteresis loop

Figure 16: Verification of the GP-NARX model for medium excitation amplitude (0.10 V) considering a swept sine test. ▒ represents the 99% model-predicted output confidence bands, — is the model response mean and • represents ten experimental realizations.

sipation is predicted compared to the experimental measurements. Besides, the hysteresis loop's asymmetry concerning the zero axes of the displacement has been well-captured by the model.

Figure 20 depicts the model's performance in reproducing the behavior of the experimental structure for a white noise input conducted over the frequency range of $0 - 110$ Hz with an amplitude level of 0.30 V. As expected, since data with random characteristics are distant from those used for model training, the more uncertain is the model's predictions. This is reflected through the larger confidence bands. Another factor contributing to the more significant uncertainty of the model is related to the influence of noise on the experimental response since the maximum response amplitude for the random input is illustrated in Fig. 20(b) is less than 2 mm. In this condition, the system still operates close to the linear regime of motion, and the mean response of the model fits

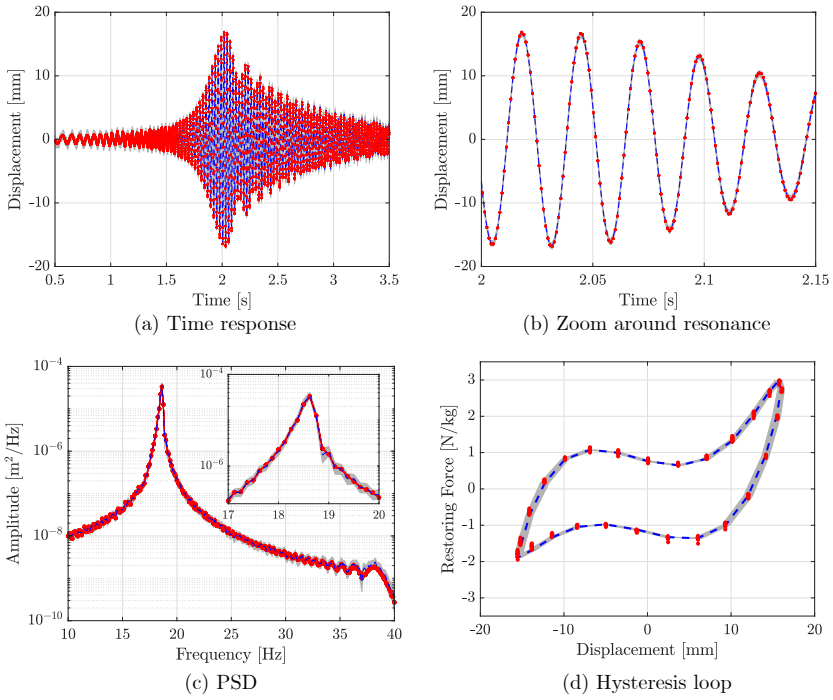

(a) Time response (b) Zoom around resonance

(c) PSD (d) Hysteresis loop

Figure 17: Verification of the GP-NARX model for high excitation amplitude (0.20 V) considering a swept sine test. ▒ represents the 99% model-predicted output confidence bands, — is the model response mean and • represents ten experimental realizations.

well the experimental realization. Figure 20(c) presents the frequency components of both signals through their estimated PSDs, showing that the identified model can adequately predict the experimental results.

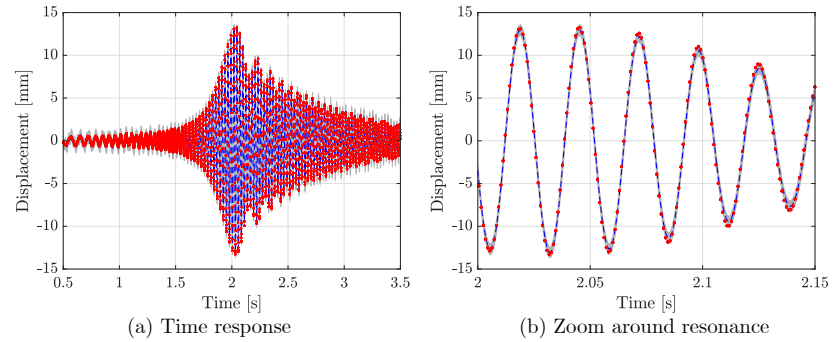

(a) Time response (b) Zoom around resonance

(c) PSD (d) Hysteresis loop

Figure 18: Validation of the GP-NARX model for medium excitation amplitude (0.15 V) considering a swept sine test. ▓ represents the 99% model-predicted output confidence bands, —— is the model response mean and • represents ten experimental realizations.

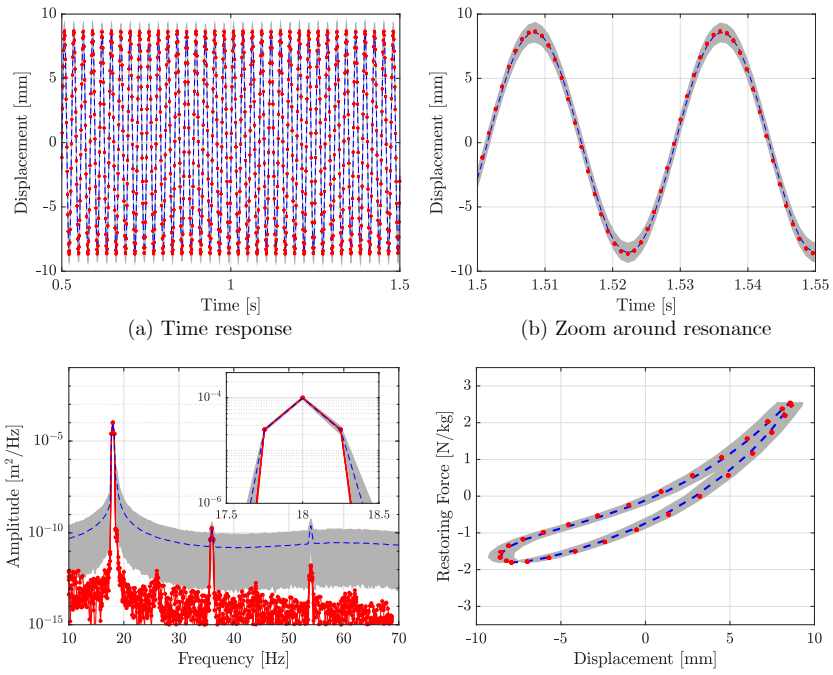

(a) Time response (b) Zoom around resonance

(c) PSD (d) Hysteresis loop

Figure 19: Validation of the GP-NARX model for a high excitation amplitude (0.15 V) considering a sinusoidal amplitude with excitation frequency at 18 Hz. ■ represents the 99% model-predicted output confidence bands, —— is the model response mean and • represents ten experimental realizations.

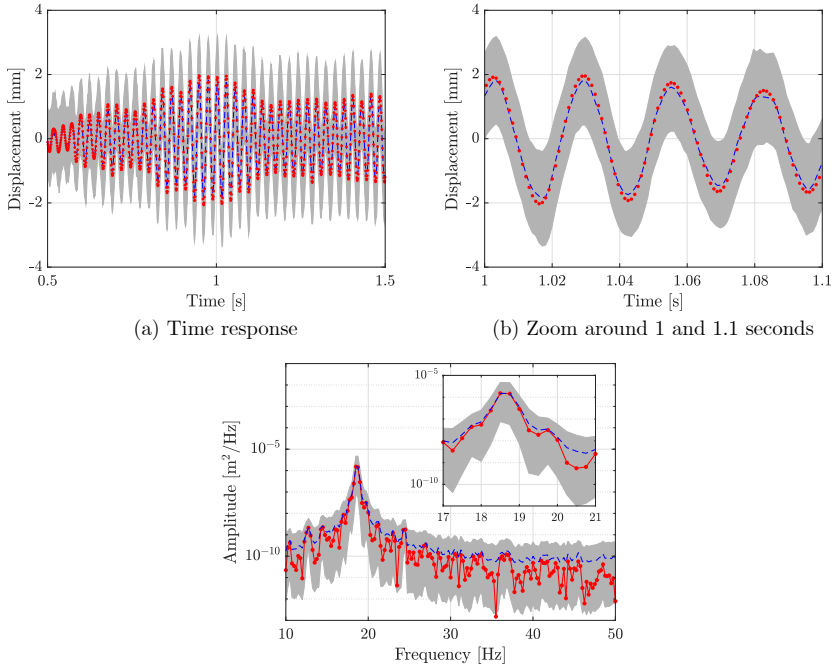

(a) Time response

(b) Zoom around 1 and 1.1 seconds

(c) PSD

Figure 20: Validation of the GP-NARX model for an excitation amplitude of 0.30 V considering a white noise input. ▓ represents the 99% model-predicted output confidence bands, — is the model response mean and • represents the experimental data.

5. Final Remarks

In this work, a GP-NARX model was used to approximate the response of nonlinear systems characterized by hysteresis effects. This work's motivation arises from the need to represent the dynamics of complex dynamic systems in several operating regimes, such as structures joined by bolted joints that experience transient and operational steady-state regimes of motion, using only input and output data to construct the model. The identification framework of the GP-NARX model was based on the steps of *data acquisition, training, verification, and validation.*

At first, attention was placed on Bouc-Wen's benchmark. The model's training to reproduce the oscillator behavior was done using swept sine tests with different excitation amplitude levels. It is argued that from these data obtained

in a transient regime around the resonant region of the system, the black-box model is trained to take into consideration the main aspects present in the dynamics of Bouc-Wen's oscillator, for example, the increase of the resonant frequency and pronounced opening of the hysteresis loops as one increases the excitation amplitudes. While the model verification was carried out assuming data of the same character as those used for training, the validation of the GP-NARX considered data originated in a different way, such as sinusoidal excitation in a steady-state regime applied at the linear resonant frequency of the system and the random phase multi-sine excitation. In contrast, in both cases, several levels of excitation amplitude were tested. Although the GP-NARX model's predictions have become more uncertain for conditions distant from the training data, the results indicate that the model has an adequate capacity to make the Bouc-Wen oscillator response predictions.

Next, the work addressed the model's performance in reproducing the BERT benchmark's behavior, taking into account uncertainties that result from the data acquisition procedure based on several experimental realizations. The experimental results were successfully correlated with predictions obtained from the GP-NARX model, assuming the available data. Further to the observations that have already been made for the numerical application case, it is encouraging to note that in addition to inferring the model prediction uncertainties, the confidence bounds can also accommodate uncertainties related to the experimental measurement process, highlighting the advantage of using the GP-NARX model.

This work paves the way to explore the GP-NARX model's use in reproducing the behavior of more complex real engineering structures involving the presence of fastened joints. The results presented exemplify the model's application for an available tightening torque applied to the experimental structure. Future work lies in exploring the use of the black-box model to reproduce the behavior of the structures with uncertainties in the measurement process for several levels of tightening torque and, from that, explore features present in the response of the GP-NARX model for structural health monitoring (SHM) purposes that aim to detect the loss of tightening torque.

Acknowledgments

The authors thank the financial support provided by Brazilian National Counsel of Technological and Scientific Development (CNPq) grant number 306526/2019-0 and São Paulo Research Foundation (FAPESP) grant numbers 15/25676-2, 16/21973-5, 17/24977-4, and 19/19684-3.

References

[1] M. R. W. Brake, D. J. Ewins, C. B. Wynn, Are Joints Necessary?, Springer International Publishing, Cham, 2018, pp. 25–36. doi:10.1007/978-3-319-56818-8_3.

[2] L. Gaul, J. Lenz, Nonlinear dynamics of structures assembled by bolted joints, Acta Mechanica 125 (1) (1997) 169–181. doi:10.1007/BF01177306.

[3] Y. Song, C. Hartwigsen, D. McFarland, A. Vakakis, L. Bergman, Simulation of dynamics of beam structures with bolted joints using adjusted Iwan beam elements, Journal of Sound and Vibration 273 (1) (2004) 249 – 276. doi:https://doi.org/10.1016/S0022-460X(03)00499-1.

[4] M. R. Brake, The Mechanics of Jointed Structures: Recent Research and Open Challenges for Developing Predictive Models for Structural Dynamics, Springer, 2017.

[5] E. Rojas, S. Punla-Green, C. Broadman, M. R. W. Brake, B. R. Pacini, R. C. Flicek, D. D. Quinn, C. W. Schwingshackl, E. Dodgen, A priori methods to assess the strength of nonlinearities for design applications, in: G. Kerschen, M. R. W. Brake, L. Renson (Eds.), Nonlinear Structures and Systems, Volume 1, Springer International Publishing, Cham, 2020, pp. 243–246.

[6] H. Festjens, G. Chevallier, J.-L. Dion, A numerical tool for the design of assembled structures under dynamic loads, International Journal of Mechanical Sciences 75 (2013) 170 – 177. doi:https://doi.org/10.1016/j.ijmecsci.2013.06.013.

[7] R. M. Lacayo, M. S. Allen, Updating structural models containing nonlinear Iwan joints using quasi-static modal analysis, Mechanical Systems and Signal Processing 118 (2019) 133 – 157. doi:https://doi.org/10.1016/j.ymssp.2018.08.034.

[8] E. Jewell, M. S. Allen, I. Zare, M. Wall, Application of quasi-static modal analysis to a finite element model and experimental correlation, Journal of Sound and Vibration 479 (2020) 115376. doi:https://doi.org/10.1016/j.jsv.2020.115376.

[9] J. Yuan, C. Schwingshackl, C. Wong, L. Salles, On an improved adaptive reduced-order model for the computation of steady-state vibrations in large-scale non-conservative systems with friction joints, Nonlinear Dynamics (2020). doi:10.1007/s11071-020-05890-2.

[10] D. Wang, C. Xu, Combination reduction dynamic analysis for complex jointed structures with local hysteresis nonlinearity, Nonlinear Dynamics 101 (1) (2020) 171–190. doi:10.1007/s11071-020-05751-y.

[11] D. D. Quinn, Modal analysis of jointed structures, Journal of Sound and Vibration 331 (1) (2012) 81 – 93. doi:https://doi.org/10.1016/j.jsv.2011.08.017.

[12] H. Festjens, G. Chevallier, J. Dion, Nonlinear model order reduction of jointed structures for dynamic analysis, Journal of Sound and Vibration 333 (7) (2014) 2100 – 2113. doi:https://doi.org/10.1016/j.jsv.2013.11.039.

[13] Q. Li, X. Jing, Fault diagnosis of bolt loosening in structures with a novel second-order output spectrum–based method, Structural Health Monitoring 19 (1) (2020) 123–141. arXiv:https://doi.org/10.1177/1475921719836379, doi:10.1177/1475921719836379.

[14] Q. Li, X. Jing, A second-order output spectrum approach for fault detection of bolt loosening in a satellite-like structure with a sensor chain, Nonlinear Dynamics 89 (1) (2017) 587–606. doi:10.1007/s11071-017-3473-6.

[15] K. Worden, C. Wong, U. Parlitz, A. Hornstein, D. Engster, T. Tjahjowidodo, F. Al-Bender, D. Rizos, S. Fassois, Identification of pre-sliding and sliding friction dynamics: Grey-box and black-box models, Mechanical Systems and Signal Processing 21 (1) (2007) 514 – 534. doi:https://doi.org/10.1016/j.ymssp.2005.09.004.

[16] K. Worden, R. J. Barthorpe, Identification of hysteretic systems using NARX models, part I: Evolutionary identification, in: T. Simmermacher, S. Cogan, L. Horta, R. Barthorpe (Eds.), Topics in Model Validation and Uncertainty Quantification, Volume 4, Springer New York, New York, NY, 2012, pp. 49–56.

[17] A. Leva, L. Piroddi, NARX-based technique for the modelling of magneto-rheological damping devices, Smart Materials and Structures 11 (1) (2002) 79–88. doi:10.1088/0964-1726/11/1/309.

[18] S. A. M. Martins, L. A. Aguirre, Sufficient conditions for rate-independent hysteresis in autoregressive identified models, Mechanical Systems and Signal Processing 75 (2016) 607 – 617. doi:http://dx.doi.org/10.1016/j.ymssp.2015.12.031.

[19] J. Noël, A. Esfahani, G. Kerschen, J. Schoukens, A nonlinear state-space approach to hysteresis identification, Mechanical Systems and Signal Processing 84 (Part B) (2017) 171 – 184, recent advances in nonlinear system identification. doi:https://doi.org/10.1016/j.ymssp.2016.08.025.

[20] A. Visintin, Differential models of hysteresis, Vol. 111, Springer Science & Business Media, 2013.

[21] S. A. Billings, Nonlinear system identification: NARMAX methods in the time, frequency, and spatio-temporal domains, John Wiley & Sons, 2013.

[22] J. Noël, M. Schoukens, Hysteretic benchmark with a dynamic nonlinearity, in: Workshop on Nonlinear System Identification Benchmarks, Brussels, Belgium, 2016, pp. 7 – 14.

[23] J. Kocijan, A. Girard, B. Banko, R. Murray-Smith, Dynamic systems identification with Gaussian processes, Mathematical and Computer Modelling of Dynamical Systems 11 (4) (2005) 411–424. arXiv:https://doi.org/10.1080/13873950500068567, doi:10.1080/13873950500068567.

[24] K. Worden, W. E. Becker, T. J. Rogers, E. J. Cross, On the confidence bounds of Gaussian process NARX models and their higher-order frequency response functions, Mechanical Systems and Signal Processing 104 (2018) 188 – 223. doi:https://doi.org/10.1016/j.ymssp.2017.09.032.

[25] M. Schoukens, P. Mattsson, T. Wigren, J. Noël, Cascaded tanks benchmark combining soft and hard nonlinearities, in: Workshop on Nonlinear System Identification Benchmarks, Brussels, Belgium, 2016, pp. 20 – 23.

[26] K. Worden, R. Barthorpe, E. Cross, N. Dervilis, G. Holmes, G. Manson, T. Rogers, On evolutionary system identification with applications to nonlinear benchmarks, Mechanical Systems and Signal Processing 112 (2018) 194 – 232. doi:https://doi.org/10.1016/j.ymssp.2018.04.001.

[27] C. K. I. Williams, C. E. Rasmussen, Gaussian processes for machine learning, Vol. 2, MIT press Cambridge, MA, 2006.

[28] E. Schulz, M. Speekenbrink, A. Krause, A tutorial on Gaussian process regression: Modelling, exploring, and exploiting functions, Journal of Mathematical Psychology 85 (2018) 1 – 16. doi:http://doi.org/10.1016/j.jmp.2018.03.001.

[29] M. Seeger, Gaussian Process for Machine Learning, International Journal of Neural Systems 14 (02) (2004) 69–106, pMID: 15112367. arXiv:https://doi.org/10.1142/S0129065704001899, doi:10.1142/S0129065704001899.

[30] C. L. C. Mattos, A. Damianou, G. A. Barreto, N. D. Lawrence, Latent Autoregressive Gaussian Processes Models for Robust System Identification, IFAC-PapersOnLine 49 (7) (2016) 1121 – 1126, 11th IFAC Symposium on Dynamics and Control of Process SystemsIncluding Biosystems DYCOPS-CAB 2016. doi:http://doi.org/10.1016/j.ifacol.2016.07.353.

[31] J. Q. Candela, A. Girard, J. Larsen, C. E. Rasmussen, Propagation of uncertainty in Bayesian kernel models - application to multiple-step ahead

forecasting, in: 2003 IEEE International Conference on Acoustics, Speech, and Signal Processing, 2003. Proceedings. (ICASSP '03)., Vol. 2, 2003, pp. 2–701. doi:10.1109/ICASSP.2003.1202463.

[32] C. P. Robert, G. Casella, Monte Carlo Statistical Methods, Springer, New York, 2010.

[33] A. Bajrić, J. Høgsberg, Estimation of hysteretic damping of structures by stochastic subspace identification, Mechanical Systems and Signal Processing 105 (2018) 36 – 50. doi:https://doi.org/10.1016/j.ymssp.2017.11.042.

[34] M. Rebillat, M. Schoukens, Comparison of least squares and exponential sine sweep methods for parallel hammerstein models estimation, Mechanical Systems and Signal Processing 104 (2018) 851 – 865. doi:https://doi.org/10.1016/j.ymssp.2017.11.015.

[35] R. O. Teloli, S. da Silva, A new way for harmonic probing of hysteretic systems through nonlinear smooth operators, Mechanical Systems and Signal Processing 121 (2019) 856–875. doi:https://doi.org/10.1016/j.ymssp.2018.11.044.

[36] L. P. Miguel, R. de Oliveira Teloli, S. da Silva, Some practical regards on the application of the harmonic balance method for hysteresis models, Mechanical Systems and Signal Processing 143 (2020) 106842. doi:https://doi.org/10.1016/j.ymssp.2020.106842.

[37] B. Bhattacharyya, E. Jacquelin, D. Brizard, A Kriging-NARX model for uncertainty quantification of nonlinear stochastic dynamical systems in

time domain, Journal of Engineering Mechanics 146 (7) (2020) 04020070. doi:10.1061/(ASCE)EM.1943-7889.0001792.

[38] T. T. Baber, Y.-K. Wen, Random vibration hysteretic, degrading systems, Journal of the Engineering Mechanics Division 107 (6) (1981) 1069–1087.

[39] F. Ikhouane, J. Rodellar, Systems with hysteresis: analysis, identification and control using the Bouc-Wen model, John Wiley & Sons, 2007.

[40] M. Peeters, G. Kerschen, J. Golinval, Modal testing of nonlinear vibrating structures based on nonlinear normal modes: Experimental demonstration, Mechanical Systems and Signal Processing 25 (4) (2011) 1227 – 1247. doi:https://doi.org/10.1016/j.ymssp.2010.11.006.

[41] R. de O. Teloli, S. da Silva, T. G. Ritto, G. Chevallier, Bayesian model identification of higher-order frequency response functions for structures assembled by bolted joints, Mechanical Systems and Signal Processing 151 (2021) 107333. doi:https://doi.org/10.1016/j.ymssp.2020.107333.

[42] L. G. G. Villani, S. da Silva, A. Cunha Jr, M. D. Todd, Damage detection in an uncertain nonlinear beam based on stochastic Volterra series: An experimental application, Mechanical Systems and Signal Processing 128 (2019) 463–478. doi:https://doi.org/10.1016/j.ymssp.2019.03.045.